Journal of Power Sources 195 (2010) 2399–2404

Contents lists available at ScienceDirect

Journal of Power Sources

journal homepage: www.elsevier.com/locate/jpowsour

Iron/carbon-black composite nanoparticles as an iron electrode material in a paste type rechargeable alkaline battery

Chen-Yu Kao*, Kan-Sen Chou

Department of Chemical Engineering, National Tsing Hua University, 101 Section 2, Kuang-Fu Road, Hsinchu 30013, Taiwan

ARTICLE INFO

Article history:
Received 11 May 2009
Received in revised form 6 August 2009
Accepted 7 August 2009
Available online 14 August 2009

Keywords:
Nanoparticles
Iron electrode
Rechargeable alkaline battery

ABSTRACT

Iron/carbon-black composite nanoparticles were synthesized by chemically reducing the iron salt mixing with carbon black by adding $NaBH_4$ in the aqueous solution. Carbon-black particles, with a mean particle size of approximately 40 nm, function as the nucleation cores for iron deposition. Additionally, core–shell iron composite particles are observed to be 30–100 nm with spherical sharp. At the first time discharge, the iron/carbon-black composite nanoparticle discharged 1200 mAh g^{-1}(Fe) at plateau one and 400 mAh g^{-1}at plateau two at a high current density of 200 mA g^{-1}(Fe). The capacity is larger than the theoretical value, which is attributed to the formation of iron hydride (FeH_x) while the iron was reduced by $NaBH_4$, followed the hydrogen reaction as an active material while the battery discharge occurs. In further cycles, the iron/carbon-black composite iron electrode shows a good reversibility of about 600 mAh g^{-1}(Fe) when the nickel–iron battery operated between 1.65 and 0.8 V. XRD analysis results indicate that the carbon black in the core of the iron/carbon-black composite enhances the reduction/oxidation reactions of iron, as achieved by the carbon black forming an enhanced electronic conductive network while iron is discharged as the insulator species such as $Fe(OH)_2$ and Fe_3O_4. SEM images reveal that the iron/carbon-black composite keeps particle sizes smaller than 300 nm during the electrode cycling, indicating that carbon black also acts as the nucleation cores for the dissolution–deposition of iron.

1. Introduction

Large scale batteries are widely discussed for use in electrical powered vehicles. Safe, low cost, and high energy density are the basic requirements of it. Of particular interest are lithium ion batteries, in which $LiFePO_4$ is used as the cathode material. Despite their attractiveness given the abundance of iron and the highly safe nature of $LiFePO_4$, lithium ion batteries are limited in safety owing to the flammable organic electrolyte contained inside. In contrast, alkaline rechargeable batteries satisfy safety concerns owing to their use of an aqueous electrolyte. The Ni–Fe rechargeable alkaline battery, in which iron is used as the anode and $Ni(OH)_2$ as the cathode material, was developed around 1900, and has a cycle life of 3000 cycles and a calendar life of about 20 years [1]. Despite its good resistance against overcharging, deep discharging, and mechanical shocks, this battery has been replaced owing to its relatively low power density, low energy density [2], and high self-discharge [3]. Alternatively, nickel–iron batteries are highly promising for large scale battery applications owing to their high theoretical capacity, inexpensiveness, and absence of toxic materials. Although the theoretical capacity of iron is 962 mAh g^{-1}, in previous studies, the iron electrode performed as low as 1/3 of the theoretical value [4–7], owing to the formation of a passive film [8]. While attempting to enhance the capacity and power density of iron active materials, our previous study [9] used the nanosized iron particle, in which the nanosized iron particle discharge capacity is about 700 mAh g^{-1}(Fe) during the first cycle, a capacity that was significantly higher than in other studies. However, the capacity of the active material decreases quickly to less than 300 mAh g^{-1} during the second or third cycle. Although other investigators made nanosized iron active materials, the reversibility was not improved [10–14]. This work describes a novel composite structure with carbon-black particle as the core and iron as the shell, via the formation of a good conductive network of carbon black to improve the reversibility of the active material.

2. Experimental

2.1. Preparation of active materials

Nanosized iron particles were synthesized by chemically reducing Fe ion by sodium borohydride. 0.025 mole of $FeSO_4{\cdot}7H_2O$

* Corresponding author. Tel.: +886 3 5715131x33657; fax: +886 3 5725924.
E-mail address: d947625@oz.nthu.edu.tw (C.-Y. Kao).

0378-7753/$ – see front matter © 2009 Elsevier B.V. All rights reserved.
doi:10.1016/j.jpowsour.2009.08.008

(Showa, Japan) was dissolved in 200 ml D.I. water, followed by dissolution of 0.05 mole of $NaBH_4$ (Lancaster, England) in 50 ml D.I. water. The $NaBH_4$ solution was then pumped into the $FeSO_4$ solution of 5 ml min^{-1} with an ice bath. Next, composite iron nanoparticles were prepared by reducing Fe on the surface of carbon-black particles. The carbon black (40 nm, Timcal, Switzerland) was pre-mixed with the $FeSO_4$ solution, followed by pumping of the $NaBH_4$ solution into the $FeSO_4$ solution of 5 ml min^{-1} with an ice bath. Additionally, all reaction solutions were stirred continuously for 30 min to complete the reduction reaction. The synthesized iron particles were then washed by hot water (~90 °C) and separated by a magnet three times. After the unwanted reactants were removed, the samples were stored in acetone to prevent oxidation. Moreover, the samples were identified by X-ray diffraction (XRD; Rigaku, Japan), and the morphology was observed by scanning electron microscopy (SEM; S-4700, Hitachi, Japan). Cyclic voltammetry studies were conducted with a three-electrode cell assembly, in which iron electrodes were used as the working electrode, and nickel hydroxide as the counter electrode, Ag/AgCl as the reference electrode. Notably, the electrolyte was 8 M KOH + 1 M LiOH aqueous solution. Finally, cyclic voltammetry measurements were recorded at a sweep rate of 5 mV s^{-1} and in the range of −0.4 to 1.4 V.

2.2. Preparation of iron electrode and cell assembling

Paste type iron electrodes were prepared to evaluate the performance of iron active materials. The synthesized iron active materials, which contained 1.39 g of iron, were mixed with 0.028 g of Na_2S (Showa, Japan) and 0.14 g of PTFE (60% suspended solution, Aldrich, USA) to form the pastes. The pastes were then poured into nickel foam current collectors (80 mm × 40 mm × 1.8 mm, 110 ppi). Next, the iron electrodes were packed by non-woven PP cloth as separators. A miniature cell was assembled with a single iron electrode and two nickel electrodes with an excess capacity placed on both side; the cell was then packed in a case. The base electrolyte in the experiment is 8 M aqueous KOH solution containing 1 M LiOH. Additionally, the performance of the iron electrodes was evaluated based on its discharge capacity. Finally, the cells were cycled in the range of 0.8–1.65 V at a current density of 200 mA g^{-1}(Fe) at room temperature by a battery automatic tester (760B, Acutech System, Taiwan).

3. Results and discussion

3.1. Characteristics of synthesized iron nanoparticles

Fig. 1 shows the XRD patterns of the reduced pure iron and iron/carbon-black composite. The XRD pattern of the reduced pure iron reveals a weak and broad peak at Fe(1 1 0), indicating that the iron is obviously reduced and has a poor crystalline structure.

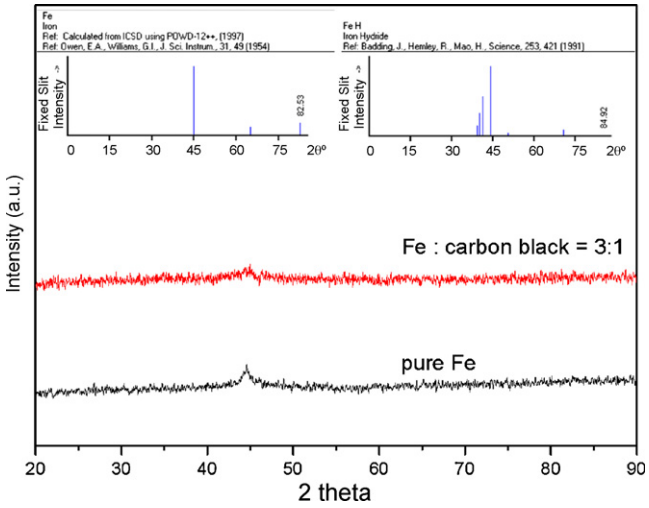

Fig. 1. XRD patterns of pure iron and iron/carbon-black composite nanoparticles as prepared.

The XRD pattern of the iron/carbon-black composite nanoparticle shows a weaker peak than that of pure iron, suggesting that the iron deposited on the surface of carbon-black particles decreases the grain size of iron.

ICP-MS analysis reveals that the boron residual in the iron particles was about 4.8 wt.% or 0.25(mol/mol) even after the samples were washed by D.I. water three times. Some studies suggest that the compound Fe_2B forms when iron is reduced by BH_4^- in an aqueous solution [15]. The reactions are shown as follows:

$$Fe^{2+}(aq) + 2BH_4^-(aq) + 2H_2O \rightarrow Fe(s) + B_2H_6 + H_2 \quad (1)$$

$$B_2H_6 + 6H_2O \rightarrow 2B(OH)_3 + 6H_2 \quad (2)$$

According to reaction (1), B_2H_6 is produced when the reduction reaction proceeded. The intermediate B_2H_6 then decomposes to B and H_2 and, then, the boron combines with iron. However, in an aqueous solution, B_2H_6 also reacts with H_2O subsequently producing $B(OH)_3$ and H_2 (Eq. (2)). Therefore, only a slight amount of Fe_2B is produced [15]. Additionally, a significant amount of hydrogen is produced during the reduction reaction, implying that the hydrogen is either trapped in the crystalline structure or adsorbed on the iron surface [16,17], subsequently forming the iron hydride (FeH_x). Comparing the XRD patterns in Fig. 1 reveals that, although the strongest peak shifts slightly to the peak of FeH (44.2°), this is not exactly the peak of pure iron. Therefore, we believe that the fresh sample of the reduction reaction closely resembles the mixture of Fe, FeH and $B(OH)_3$.

Fig. 2 shows the SEM images of these two iron particles. In Fig. 2(a), the pure iron particles strongly aggregate together and their particle sizes range from 50 to 150 nm. In contrast, the particle

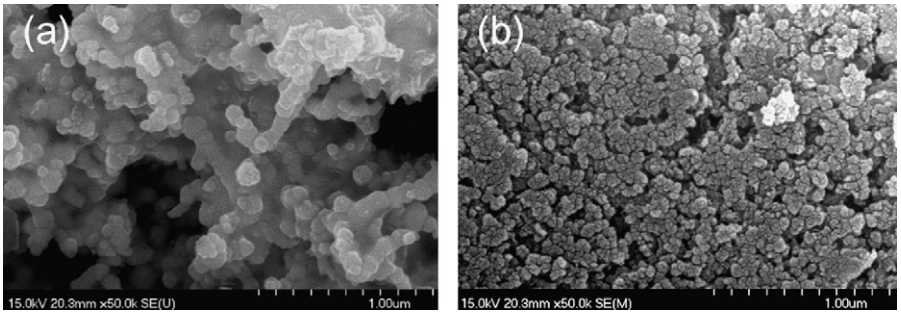

Fig. 2. SEM images of the iron nanoparticles as prepared: (a) pure iron and (b) iron/carbon-black composite.

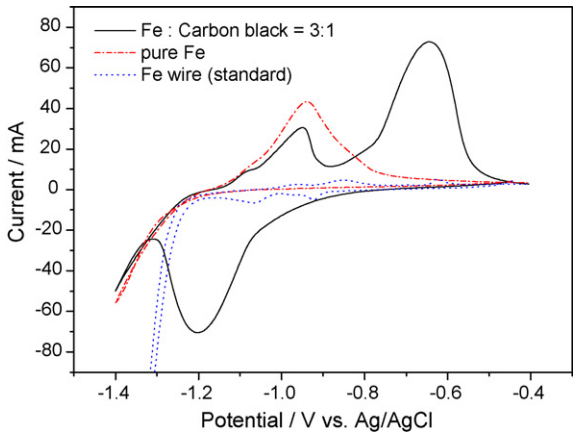

Fig. 3. Cyclic voltammetry of iron electrode materials in 8 M KOH + 1 M LiOH solution.

sizes of iron/carbon-black composite range from 30 to 80 nm with less aggregation, as shown in Fig. 2(b). Obviously, the carbon black changes the behavior of iron deposition, in which the carbon-black particles function as the nucleation cores and the iron deposits on the surface of carbon black, subsequently forming the core–shell structure. The measured BET surface area of the carbon black is about 25 $m^2\,g^{-1}$. When the weight ratio of iron to carbon black is 3:1, the thickness of iron on carbon-black surface is about 15 nm; in addition, the mean particle size of the iron/carbon-black composite particles is about 70 nm based on calculations, which is similar to the particles shown in Fig. 2(b). The other samples of weight ratio of iron to carbon black 5:1 and 10:1 are also prepared, in which the thicknesses of iron deposited on the carbon-black surface are about 24 and 48 nm, respectively.

Fig. 3 shows the cyclic voltammograms of the iron electrodes. The pure iron wire is used as the standard for comparison with the nanosized iron. The cyclic voltammogram of the pure iron nanoparticle only reveals a large oxidation peak of Fe/Fe(II) at around −0.94 V, The reaction can be expressed as:

$$Fe + 2OH^- \rightarrow Fe(OH)_2 + 2e^-, \qquad E^\circ = -0.87\,V \tag{3}$$

No oxidation peak of Fe(II)/Fe(III) and reduction peak of Fe/Fe(II) and Fe(II)/Fe(III) are observed, indicating not only that Fe(II) barely oxidizes to Fe(III), but also that the reversibility of Fe/Fe(II) is insufficient in the electrode material.

According to the cyclic voltammogram of the iron/carbon-black composite, an oxidation peak appears at around −0.95 V and a larger oxidation peak appears at −0.64 V. The first oxidation peak is the same as that in reaction (3), while the second oxidation peak corresponds to the Fe(II) oxide to Fe(III). The possible reactions are expressed as [6]:

$$3Fe(OH)_2 + 2OH^- \rightarrow 2e^- + Fe_3O_4 + 4H_2O, \qquad E^\circ = -0.66\,V \tag{4}$$

or

$$Fe(OH)_2 + OH^- \rightarrow FeOOH + H_2O + e^-, \qquad E^\circ = -0.56\,V \tag{5}$$

The cyclic voltammogram shows only one reduction peak from −1.0 to −1.3 V, possibly due to the reduction peaks of Fe/Fe(II) and Fe(II)/Fe(III) merged as one broad peak. The strong oxidation and reduction peaks of the cyclic voltammogram of the iron/carbon-black composite nanoparticles imply their high reversibility at a high current density.

3.2. Performance of nanosized iron materials

Fig. 4 shows the discharge curves of the nanosized iron particle as well as the iron/carbon-black composite nanoparticle. In Fig. 4(a),

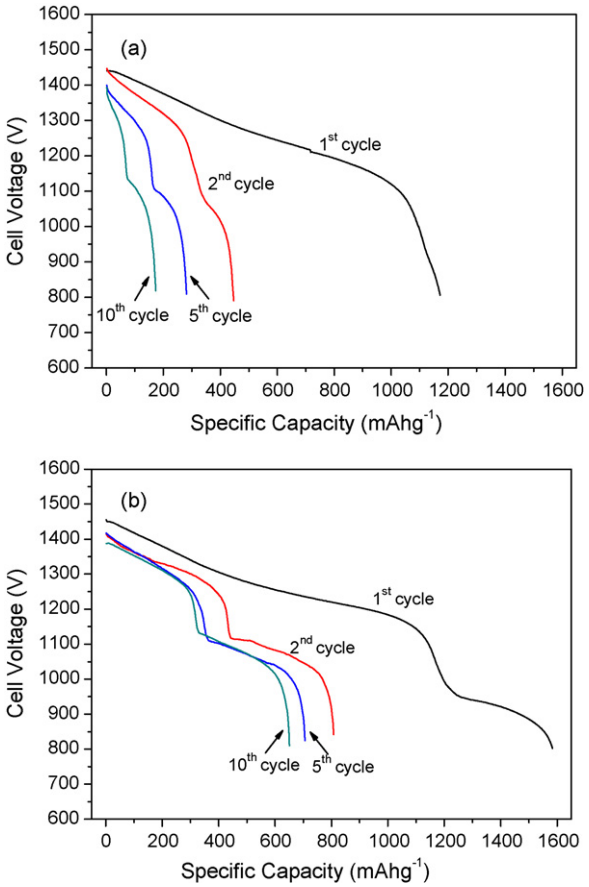

Fig. 4. Discharge curves of the nickel–iron battery: (a) pure iron nanoparticle and (b) iron/carbon-black composite nanoparticle a constant current 200 mA g^{-1} was applied at 25 °C.

the first time discharge curve shows only one plateau that corresponds to the reaction in which Fe oxidizes to $Fe(OH)_2$; in addition, the discharged capacity is about 1200 mAh g^{-1}(Fe). The capacity exceeds the theoretical capacity of iron (962 mAh g^{-1}), indicating that the discharge does not only involve the oxidation of iron. Boron is an element involved in iron nanoparticles from ICP-MS analysis. Although the reduction potential of Boron in alkali electrolyte is $E^\circ = -1.79$ V, such a high voltage plateau is not observed in the discharge curves. However, the XRD examination indicates that the reactants of the reduction reaction might include the iron hydride (FeH_x). If so, when the iron electrode is discharged, the iron reacts to $Fe(OH)_2$ and the hydrogen reacts with OH^- and produces H_2O. The reduction potential of hydrogen in the alkali electrolyte is $E^\circ = -0.83$ V, which is very close to the potential of Fe to Fe(II) ($E^\circ = -0.87$ V). Therefore, the discharge curves of these two reactions may not be divided clearly. Moreover, the discharged capacity of the iron nanoparticle is approximately 1.25 times higher than that of the theoretical value; therefore, the ratio of H/Fe is about 0.5. The same as shown in the cyclic voltammograms, the second discharge step of the pure iron electrode is not observed, as possibly owing to the poor transmission of the electrons. The electrons move from an anode material to a cathode material via an electric conductive connection when the battery discharges. However, if all of the Fe become $Fe(OH)_2$, the nanoparticles lose the conductive connection with the current collect, no electrons can be transmitted and, ultimately, the second discharge reaction stops. Fig. 4(a) also shows the discharge curves of the pure iron nanoparticle electrode during further cycles. During the second cycle, although the second discharge plateau is observed, the capacity that combines both two

plateaus dramatically decreases to 450 mAh g^{-1}(Fe). During the 10th cycle, the discharge capacity is only 180 mAh g^{-1}(Fe). Obviously, the pure iron nanoparticle has extremely poor cycle ability. The capacity dramatically decreases during the second cycle due to the FeH_x irreversibly oxidized. During the first time discharge, the Fe oxidizes to Fe(II) and hydrogen oxidizes to H_2O individually. During the subsequent charge, the Fe(II) is reduced to Fe ($E^\circ = -0.87$ V) first, and then H_2 ($E^\circ = -0.83$ V) is produced on the surface of iron particle due to the hydrogen over potential. Owing to that less of H_2 is produced and the iron particle surface decrease, the adsorption of H_2 by iron is much less than that in iron nanoparticles reduced by $NaBH_4$.

Fig. 4(b) shows the discharge curve of the iron/carbon-black composite, in which both plateau one and plateau two are shown at the first time discharge; in addition, the discharged capacity is about 1200 mAh g^{-1}(Fe) and 400 mAh g^{-1}, respectively. The second step reaction of iron involves electrons transfer from the $Fe(OH)_2$ to the current collect. The high discharge capacity of the second step indicates that the carbon-black particles as cores of the iron composite obviously form a good electric conductive network, while all of the iron reacts as the non-conductor. At further cycles, both plateaus are clearly shown, and the capacity fading is not as quickly as that of pure iron nanoparticle electrode. The capacity during the second cycle is 820 mAh g^{-1}(Fe) and, during the 10th cycle, it is 630 mAh g^{-1}(Fe) when the nickel–iron battery operates between 1.65 and 0.8 V.

The reactants in iron electrodes are also examined by XRD analyses. In Fig. 5, the XRD pattern of the reactants of the pure iron nanoparticle electrode discharged to the cell voltage of 0.8 V shows weak peaks of iron and FeOOH. Most of the composition of this sample is $Fe(OH)_2$ by observation, and it is not easily detected by XRD analysis due to its amorphous structure. The FeOOH presented is due to $Fe(OH)_2$ easily oxidizes to Fe(III) during the sample preparation. Conversely, when the iron/carbon-black composite is discharged to the cell voltage of 0.8 V, XRD analysis reveals only strong peaks of Fe_3O_4; in addition, almost no iron is retained. This finding suggests that satisfactory conduct network is essential for Fe(II)/Fe(III) reaction. This finding also demonstrates that the second discharge step of the iron electrode is reaction (4).

Fig. 6 presents the capacity retention of the pure iron and iron/carbon-black composite samples. For all samples, the capacity decreases quickly during the initial few cycles, tending to stabilize after ten cycles. The pure iron nanoparticle shows extremely poor capacity retention; during the 40th cycle, the discharge capacity is only about 100 mAh g^{-1}(Fe). Adding the carbon black of 1/10(wt/wt) of iron slightly improves the capacity retention. Additionally, increasing the carbon black to 1/5(wt/wt) of iron significantly enhances the capacity retention, i.e. the value is 480 mAh g^{-1}(Fe) during the 40th cycle. When the carbon black is increased to 1/3(wt/wt) of iron the iron/carbon-black composite electrode has a capacity of about 600 mAh g^{-1}(Fe) during the 40th cycle; in addition, the capacity fading is slow. This finding suggests that a higher quantity of carbon black in active material discharges a higher specific capacity of iron. However, carbon black decreases the weight ratio of iron in an active material. Therefore, adding too much carbon black may decrease the specific capacity based on all materials. In this work, the quantity of carbon black of 1/3(wt/wt) of iron shows the best performance, and 1/5(wt/wt) of iron is the minima value. This finding reveals nearly no improvement of the capacity retention after adding a slight amount of carbon black in iron composite, possibly owing to that the overly thick layer of Fe(II) or Fe(III) covers the carbon-black surface, subsequently preventing the transmission of electrons between carbon black and carbon black. Although some studies have demonstrated that electrons can transmit through the insulator by the tunneling effect, the allowed distance between two conductors is only several nm [18] which depends on the insulator species. In this work, iron is coated on the surface of carbon black; once discharged, the carbon black is covered by an insulator layer such as Fe(II) or Fe(III). Therefore, too low of a fraction of carbon black implies too thick of an insulator shell, ultimately preventing the transmission of electrons via the tunneling effect.

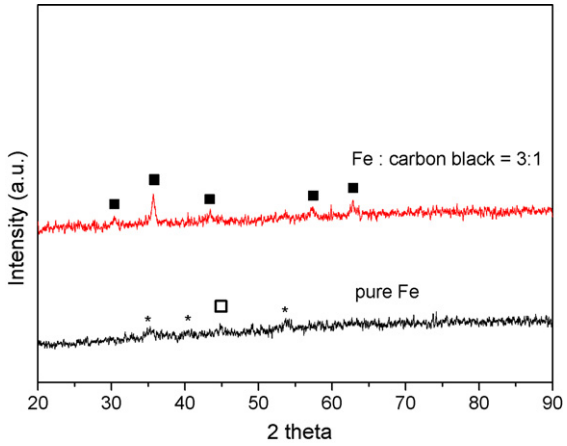

Fig. 5. XRD patterns of pure iron and iron/carbon-black composite nanoparticles discharged to a cell voltage of 0.8 V (□, Fe; ■, Fe_3O_4; *, FeOOH).

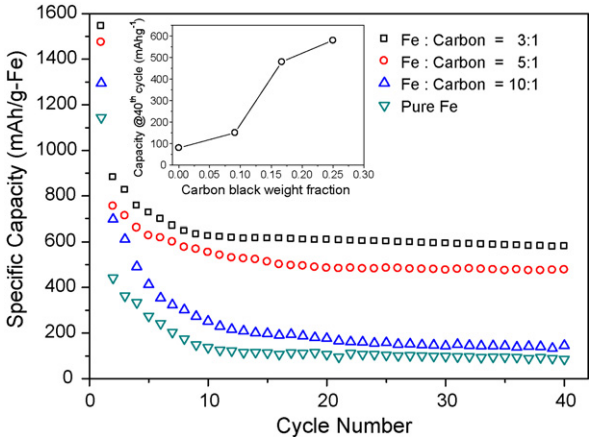

Fig. 6. Cycling stability curves of various iron electrode materials at a current density of 200 mA g^{-1} between 1.65 and 0.8 V.

Fig. 7 presents the SEM images of pure iron nanoparticle and iron/carbon-black composite nanoparticle electrode after 20 discharge/charge cycles. In Fig. 7(a), most particles of the pure iron nanoparticle electrode become larger than 100 nm. Meanwhile, some of the particles become as large as 1 μm, subsequently decreasing the ability for a high rate discharge. Conversely, the iron/carbon-black composite electrode maintains a small particle size and no particle larger than 300 nm is observed. The particle size grows via the dissolution–deposition process of iron. The soluble intermediate $HFeO_2^-$ forms when the iron active material is at the discharge state. The reaction is shown as [6]:

$$Fe(OH)_2 + OH^- \leftrightarrow HFeO_2^- + H_2O \quad (6)$$

The iron deposited from the dissolved iron species is like an electroplating process. When the iron electrode is charged, the dissolved $HFeO_2^-$ deposits on the surface where supplying electrons. Inside the pure iron nanoparticle electrode, the electric conductive connection between particle and particle is unacceptable at the dis-

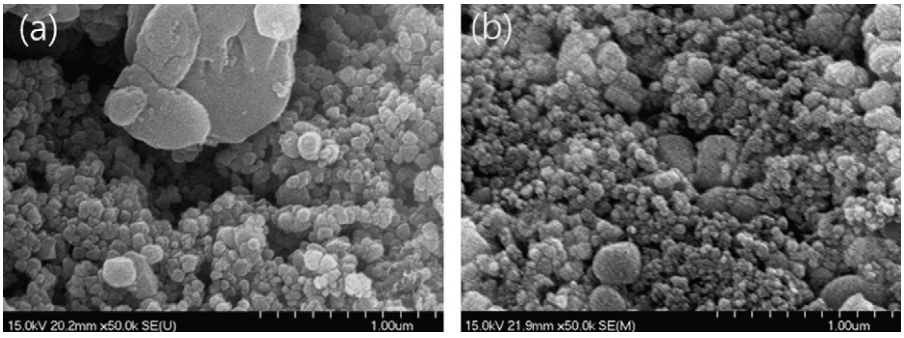

Fig. 7. SEM images of the iron nanoparticles after 20 cycles at charge state: (a) pure Fe and (b) Fe:carbon black = 3:1.

charge state. Therefore, the iron deposits only on a small area near the current collector and consequently some of the particles grow gradually and some of the particles always remain in the discharge state.

Fig. 8(a) presents the XRD patterns of pure iron nanoparticle electrode at the charge and discharge states after 20 cycles. According to this figure, even at the charge state, Fe_3O_4 is detected and the peak of iron is very weak. At discharge state, the XRD pattern reveals that some of the iron still does not react to Fe(II). This finding suggests that some of the iron is isolated. In contrast, the iron/carbon-black composite nanoparticle reveals extremely strong iron peaks at the charge state and shows strong Fe_3O_4 peaks at the discharge state in Fig. 8(b). We can infer that the electrons transferring from particle to particle are uninhibited to extent that the iron/carbon-black composite nanoparticle can be discharged from Fe to Fe_3O_4 and easily charged from Fe_3O_4 to Fe. Therefore, the dissolved intermediate deposits on most particles uniformly, subsequently, reducing particle growth.

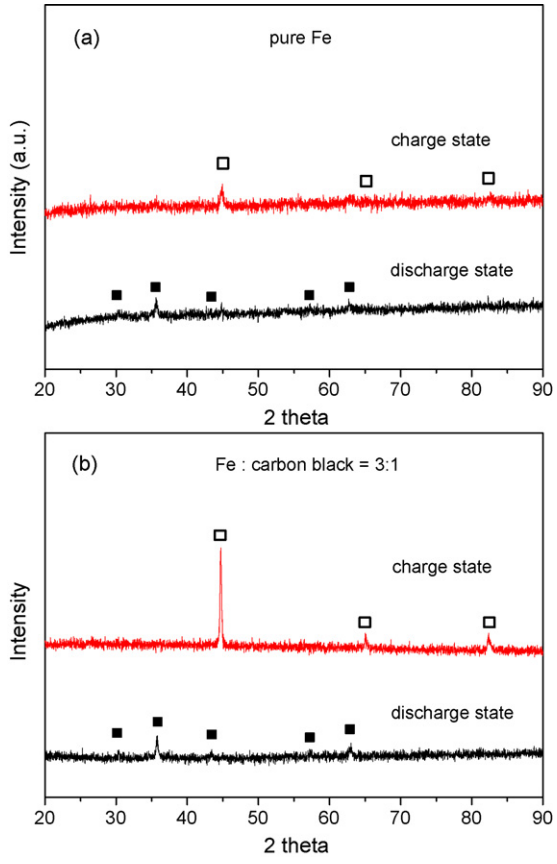

Fig. 8. XRD patterns of iron electrode materials at charge and discharge states after 20 cycles: (a) pure iron and (b) iron/carbon-black composite nanoparticles (□, Fe; ■, Fe_3O_4).

4. Conclusions

A high reversibility iron active material was prepared successfully by chemically reducing iron on carbon-black surface. During the first time discharge, the iron electrode discharged as high as 1200 mAh g^{-1}(Fe) at plateau one and 400 mAh g^{-1}(Fe) at plateau two at a high current density of 200 mA g^{-1}(Fe). A capacity exceeding the theoretical value is attributed to formation of the iron hydride during the iron composite reduced by $NaBH_4$. The hydrogen in iron structure is also discharged as an active material. During the subsequent cycles, the iron electrode exhibited good cycle performance; the stable capacity was 600 mAh g^{-1}(Fe) when it operated between 1.65 and 0.8 V. The high reversibility of the iron composite was due to the carbon black forming a good electric conductive network while the iron was discharged as the non-conductor such as $Fe(OH)_2$ or Fe_3O_4. The carbon black also acts as the nucleation cores for depositing the dissolved iron intermediate, subsequently preventing the iron particle size from growth during the charge/discharge cycles and maintaining the ability of a high rate discharge.

Acknowledgment

The authors would like to thank National Science Council of the Republic of China, Taiwan, for financially supporting this research under Contract No. NSC 96-2628-E007-022MY3.

References

[1] A.K. Shukla, S. Venugopalan, B. Hariprakash, J. Power Sources 100 (2001) 125.
[2] P. Periasamy, B.R. Babu, S.V. Iyer, J. Power Sources 62 (1996) 9.
[3] C.A.C. Souza, I.A. Carlos, M. Lopes, G.A. Finazzi, M.R.H. de Almeida, J. Power Sources 132 (2004) 288.
[4] D. Yamashita, Y. Yamamoto, K. Masuse, H. Yoshida, Nippon Kagaku Kaishi (1978) 525.
[5] C. Chakkaravarthy, P. Periasamy, S. Jegannathan, K.I. Vasu, J. Power Sources 35 (1991) 21.
[6] A.K. Shukla, M.K. Ravikumar, T.S. Balasubramanian, J. Power Sources 51 (1994) 29.
[7] M.K. Ravikumar, T.S. Balasubramanian, A.K. Shukla, J. Power Sources 56 (1995) 209.
[8] W.C. He, H.B. Shao, Q.Q. Chen, J.M. Wang, J.Q. Mang, Acta Phys. Chim. Sin. 23 (2007) 1525.
[9] K.C. Huang, K.S. Chou, Electrochem. Commun. 9 (2007) 1907.
[10] B.T. Hang, M. Eashira, I. Watanabe, S. Okada, J.I. Yamaki, S.H. Yoon, I. Mochida, J. Power Sources 143 (2005) 256.
[11] B.T. Hang, H. Hayashi, S.H. Yoon, S. Okada, J. Yamaki, J. Power Sources 178 (2008) 393.
[12] B.T. Hang, T. Watanabe, M. Eashira, S. Okada, J. Yamaki, S. Hata, S.H. Yoon, I. Mochida, J. Power Sources 150 (2005) 261.

[13] B.T. Hang, T. Watanabe, M. Eashira, I. Watanabe, S. Okada, J. Yamaki, Electrochem. Solid State Lett. 8 (2005) A476.
[14] K. Ujimine, A. Tsutsumi, J. Power Sources 160 (2006) 1431.
[15] G.N. Glavee, K.J. Klabunde, C.M. Sorensen, G.C. Hadjipanayis, Inorg. Chem. 34 (1995) 28.
[16] D.E. Jiang, E.A. Carter, Surf. Sci. 547 (2003) 85.
[17] W. Moritz, R. Imbihl, R.J. Behm, G. Ertl, T. Matsushima, J. Chem. Phys. 83 (1985) 1959.
[18] N. Hu, Y. Karube, C. Yan, Z. Masuda, H. Fukunaga, Acta Mater. 56 (2008) 2929.